Assessing the Atmospheric Response to Subgrid Surface Heterogeneity in CESM2

Megan D. Fowler[1], Richard B. Neale[1], Jason S. Simon[2,3], David M. Lawrence[1], Nathaniel W. Chaney[2], Paul A. Dirmeyer[4], Vincent E. Larson[5,6], Meng Huang[6], and John Truesdale[1]

[1] National Center for Atmospheric Research, Boulder, CO, USA

[2] Duke University, Durham, NC, USA

[3] Saint Augustine's University, Raleigh, NC, USA

[4] George Mason University, Fairfax, VA, USA

[5] University of Wisconsin-Milwaukee, Milwaukee, WI, USA

[6] Pacific Northwest National Laboratory, Richland, WA, USA

Corresponding author: Megan D. Fowler (mdfowler@ucar.edu)

Key Points:

- A new method of conveying information on subgrid-scale surface heterogeneity to the atmosphere is introduced to CESM2.
- A comparison with large-eddy simulations suggests that the atmospheric response to heterogeneity in CESM2 is too vertically constrained.
- Future model development efforts should focus on representing heterogeneity in ways that can explicitly capture secondary circulations.

Abstract

Land-atmosphere interactions are central to the evolution of the atmospheric boundary layer and the subsequent formation of clouds and precipitation. Existing global climate models represent these connections with bulk approximations on coarse spatial scales, but observations suggest that small-scale variations in surface characteristics and co-located turbulent and momentum fluxes can significantly impact the atmosphere. Recent model development efforts have attempted to capture this phenomenon by coupling existing representations of subgrid-scale (SGS) heterogeneity between land and atmosphere models. Such approaches are in their infancy and it is not yet clear if they can produce a realistic atmospheric response to surface heterogeneity. Here, we implement a parameterization to capture the effects of SGS heterogeneity in the Community Earth System Model (CESM2), and compare single-column simulations against high-resolution Weather Research and Forecasting (WRF) large-eddy simulations (LESs), which we use as a proxy for observations. The CESM2 experiments increase the temperature and humidity variances in the lowest atmospheric levels, but the response is weaker than in WRF-LES. In part, this is attributed to an underestimate of surface heterogeneity in the land model due to a lack of SGS meteorology, a separation between deep and shallow convection schemes in the atmosphere, and a lack of explicitly represented mesoscale secondary circulations. These results highlight the complex processes involved in capturing the effects of SGS heterogeneity and suggest the need for parameterizations that communicate their influence not only at the surface but also vertically.

Plain Language Summary

Land surface temperature and soil moisture are known to influence the daily evolution of the overlying atmosphere and the formation of clouds and rainfall. While global climate models represent these interactions on relatively coarse spatial scales (i.e., 100 km or greater), smaller scale differences in surface characteristics are increasingly recognized for their ability to impact the atmosphere. Here, we implement a new feature in a climate model that communicates information on small-scale surface differences from the land to the atmospheric model. We compare the results of this addition against a high-resolution model that has previously been used to isolate the impacts of surface flux gradients, with the latter serving as a proxy for observations. Though there are some encouraging signs of the implemented approach to drive an atmospheric response to surface variability, we find that a missing representation of large-scale circulations between warm/cool surfaces likely limits model agreement.

1 Introduction

The land surface has a well-documented ability to influence planetary boundary layer (PBL) characteristics (Avissar & Pielke, 1989; Brunsell et al., 2011; H. Huang & Margulis, 2013; Hubbe et al., 1997; Kustas & Albertson, 2003; Mahrt, 2000), clouds and precipitation (Berg & Stull, 2005; Kang, 2016; Pielke Sr., 2001; Rieck et al., 2014; Schrieber et al., 1996), and hydrometeorological extremes (Fischer et al., 2007; Hirschi et al., 2011; Mocko et al., 2021; Santanello et al., 2015; Dirmeyer et al., 2021). Even relatively small scale surface features create important temperature and moisture gradients, such as between rivers/lakes and adjacent land (Ramos da Silva et al., 2011; Y. Zhang et al., 2021), or between urban and rural regions (Hjelmfelt, 1982; Baik et al., 2001; Dixon and Mote, 2003; Shepherd, 2005; Shem and Shepherd, 2009); those contrasts are often enough to drive a convective response. The horizontal scale at

which land-atmosphere interactions occur can thus be finer than what is resolved by relatively coarse global climate models (GCMs) with resolutions ≥100 km. A critical challenge for Earth system modeling has been how to represent the atmospheric impacts of such small-scale surface heterogeneity (Bou-Zeid et al., 2020; Schrieber et al., 1996).

A common strategy for representing subgrid-scale (SGS) surface heterogeneity ($\mathcal{O}(1)$- $\mathcal{O}(10)$ km) within land models has been to use a tiling approach, where each gridcell contains a statistical representation of the land cover types within it (e.g., urban, forested, etc.). Each tile is then characterized by unique surface fluxes/states that contribute to the grid-mean average based on the percent of gridcell area it covers. Avissar and Pielke (1989) proposed this approach after noting the role that differences in sensible heat flux played on PBL development, and subsequent studies have found substantial improvements when using this approach (Koster & Suarez, 1992; Hahmann & Dickinson, 2001; Dai et al., 2003; Li et al., 2013). This is especially critical at the current spatial scales of GCMs (i.e., 50-100 km), where variations in land cover are almost guaranteed within a single gridcell.

A tiling scheme as described above represents SGS surface heterogeneity within a land model, but it continues to pass only grid-mean surface fluxes to the atmosphere. From an atmospheric perspective then, any information on SGS heterogeneity in surface forcing is lost. Several studies, however, highlight the importance of this information in the development of clouds and rainfall. Berg and Stull (2005) suggest that the formation of boundary layer cumulus clouds can be tied directly to a joint probability density function (PDF) of virtual potential temperature and water vapor mixing ratio over a heterogeneous surface. Others have highlighted the ability of horizontal gradients in surface fluxes, temperature, and soil moisture to generate secondary circulations that redistribute energy and moisture (Ookouchi et al., 1984; Doran et al., 1995; Avissar & Schmidt, 1998; Bou-Zeid et al., 2020; Cheng et al., 2021). Those circulations play a key role in cloud and rainfall development (Cheng et al., 2021; Graf et al., 2021; Taylor et al., 2011; Avissar & Liu, 1996).

A recent LES study was designed to directly assess the importance of representing SGS heterogeneity by specifying surface boundary conditions that either allow for varying surface fluxes or are constant across the domain (Simon et al., 2021). Allowing surface fluxes to vary spatially was found to increase domain-average turbulence and cloud liquid water path by helping to organize convection and precipitation. Gradients in surface fluxes within a single 100 km domain can therefore generate mesoscale secondary circulations capable of altering the grid-mean environment (Simon et al., 2021).

Recent GCM-based studies have attempted to move beyond a reliance on gridcell means by exploring mechanisms that link existing parameterizations of SGS variability. M. Huang et al. (2022), hereafter H22, introduced such a scheme into the Energy Exascale Earth System Model version 1 (E3SMv1). The approach utilizes the turbulence and boundary layer scheme, Cloud Layers Unified By Binormals (CLUBB; Golaz et al., 2002; Larson et al., 2002), which estimates near-surface temperature and humidity variances and their covariance from grid-mean fluxes. To capture SGS surface heterogeneity, H22 added a term to CLUBB's boundary conditions to represent the differences in temperature and moisture present across SGS surface tiles. Single-column experiments at the Department of Energy's Atmospheric Radiation Measurement (ARM) Southern Great Plains (SGP) site during the summer of 2015 suggested that the addition drives a

slight increase in liquid water path on non-precipitating days. This is qualitatively in agreement with the results of Simon et al. (2021), but it remains to be seen how such a parameterization verifies against similar LES experiments. Although LESs are not perfect proxies for observations, the model framework established by Simon et al. (2021) allows a direct comparison between identical atmospheric conditions when treating the surface as homogeneous vs. heterogeneous. We thus consider it a reasonable approximation for how the atmosphere responds to SGS heterogeneity.

In this study, we implement a similar approach to what was used in H22 to convey information on SGS surface heterogeneity to the atmosphere within the Community Earth System Model (CESM2). The two models have similar physics in both the atmosphere and land model components, though here we also enable interactive coupling between the land and atmosphere during model run-time. More importantly, rather than investigating the ability of this parameterization to impact the atmosphere as in H22, we focus instead on the parameterization's ability to drive a similar atmospheric response to SGS heterogeneity as is present in a matching set of Weather Research and Forecasting (WRF) LES simulations. A set of single-column experiments are conducted at the SGP site to conduct this evaluation, with details on the methodology and experiment setup provided in Section 2. In Section 3, we explore the response to heterogeneity in these experiments and evaluate the signal relative to WRF-LES. We conclude in Section 4 with a summary of the main results from this analysis and their broader implications.

2 Methods

2.1 Representing surface heterogeneity in CESM2

As in E3SMv1, the CESM2 atmosphere and land models contain separate representations of SGS heterogeneity. In the Community Atmosphere Model (CAM6), this is again through CLUBB, which assumes a joint PDF to predict means and higher-order moments of liquid water potential temperature (θ_l), total water specific humidity (q_t), and vertical velocity (w). The parameters of this joint PDF depend on the grid-mean values of those fields ($\overline{\theta_l}, \overline{q_t}, \overline{w}$), their SGS variances ($\overline{\theta_l'^2}$, $\overline{q_t'^2}$, $\overline{w'^2}$) and covariances ($\overline{\theta_l' q_t'}$, $\overline{w' q_t'}$, $\overline{w' \theta_l'}$), and higher-order moments. The latter includes the skewness of vertical velocity ($\overline{w'^3}$) to represent the asymmetry of turbulent updrafts/downdrafts in CLUBB, which is explicitly represented in WRF-LES. In this notation, overbars denote grid-mean values and primes indicate SGS values (i.e., departures from the grid mean). Third and fourth order moments are found from individual closure assumptions.

Importantly, not all higher-order moments are computed at each vertical level. CLUBB is implemented on a staggered grid such that the level interfaces (vs. midpoints) only compute the second-order moments. At the lowest model level interface, assumed to be in contact with the surface, the primary focus is on the (co)variances of temperature and humidity since $\overline{w}$ is assumed to be zero. We follow the original formulation laid out in André et al. (1978) to compute these in CLUBB (i.e., the flag l_andre_1978 is set to true within CLUBB):

$$\overline{\theta_l'^2}_{HOM} = \frac{Q_o^2}{u_*^2}\left[4(1-8.3\zeta)^{\frac{2}{3}}\right] \quad \zeta < 0 \qquad = \frac{Q_o^2}{u_*^2}[4] \quad \zeta > 0 \tag{1}$$

$$\overline{q_t'^2}_{HOM} = \frac{H_o^2}{u_*^2}\left[4(1-8.3\zeta)^{\frac{2}{3}}\right] \quad \zeta < 0 \qquad = \frac{H_o^2}{u_*^2}[4] \quad \zeta > 0 \tag{2}$$

$$\overline{\theta_l' q_t'}_{HOM} = \sqrt{\overline{\theta_l'^2}}\sqrt{\overline{q_t'^2}} \tag{3}$$

Where u_* is the friction velocity, ζ is the Monin-Obukhov stability parameter, Q_0 (H_0) is the kinematic heat (moisture) flux. The subscript HOM indicates that these moments are computed assuming a homogeneous surface; that is, they depend only on grid-mean fluxes that are passed to CAM6 from the surface model. These second order moments are currently computed within CLUBB, but computing them in the surface model instead would make additional information on tile-level characteristics readily available.

The Community Land Model (CLM5; Lawrence et al., 2019) represents SGS land heterogeneity with a tiling approach, statistically dividing the area of each gridcell between different surface types. The version of CLM5 used here prescribes vegetation phenology and has no active biogeochemical component, resulting in 17 surface types that include urban areas, lakes, glaciers, bare soil, various plant functional types, and irrigated and rain-fed crops. Each surface tile is characterized by unique near-surface temperature, humidity, surface fluxes, friction velocity, and stability parameter values. These calculations use grid-mean quantities from the lowest model level of the atmosphere, either directly (e.g., temperature) or indirectly (e.g., 10-m wind speed). There is therefore no accounting for SGS meteorology at the land surface.

Building on theory proposed in Machulskaya and Mironov (2018), H22 added a new connection between near-surface CLUBB (co)variances and surface tiling schemes. The essence of the approach stems from the assumption that any grid-mean variable can be represented as the sum of two parts: the mean value and the SGS fluctuations around that mean. This is applied to the higher-order moments above as follows:

$$\overline{\theta_l'^2}_{HET} = \overline{\theta_l'^2}_{HOM} + \overline{(\theta_{l,tile} - \bar{\theta}_l)^2} \tag{4}$$

$$\overline{q_t'^2}_{HET} = \overline{q_t'^2}_{HOM} + \overline{(q_{t,tile} - \bar{q}_t)^2} \tag{5}$$

$$\overline{\theta_l' q_t'}_{HET} = \overline{\theta_l' q_t'}_{HOM} + \overline{(\theta_{l,tile} - \bar{\theta}_l)(q_{t,tile} - \bar{q}_t)} \tag{6}$$

The heterogeneous representation of these moments is thus the sum of the homogeneous calculation and the departure of each tile's temperature and humidity from the grid-mean value. The most efficient way to incorporate the heterogeneous term is to move the calculation of CLUBB's boundary conditions into CLM5. Thus the values of $\overline{\theta_l'^2}$, $\overline{q_t'^2}$, and $\overline{\theta_l' q_t'}$, along with $\overline{w'^2}, \overline{u'^2}$ and $\overline{v'^2}$ are computed from tile-level data in the land model (with or without an additional heterogeneous term) and averaged to the gridcell level before being passed to CAM6 for use in CLUBB.

2.2 Modeling Experiments

We examine the impact of this parameterization in single-column atmospheric model experiments (SCAM6; Gettelman et al., 2019) at the ARM SGP site, with the distribution of surface tiles described in Table 1. A set of control experiments follow the homogeneous approach of computing surface moments (HOM) and are compared with a set of experiments that use the new heterogeneous approach (HET). In all SCAM experiments, we increase the atmospheric vertical resolution from 32 to 64 levels in order to better resolve PBL processes. The coupling frequency between the land and atmosphere is also decreased from 20 to 5 minutes. The simulations prescribe the horizontal winds and temperature/moisture advection from the LASSO VARANAL dataset (Gustafson et al., 2019), a coarsened version of the same large-scale forcing that was used in Simon et al. (2021). Though not quite identical to the WRF-LES boundary forcing as a result of fewer vertical levels, the two are indeed similar. There is thus little reason to suspect that this is a primary driver of potential model disagreement, given the other pathways by which SCAM and WRF-LES diverge (i.e., convection and microphysical schemes, land surface models, etc.). Surface fields (i.e., surface fluxes, near-surface temperature and humidity, etc.) are allowed to evolve freely. SCAM is run at a T42 (~2.8˚) resolution, with SGS surface tile distributions defined at the same resolution.

Table 1: Distribution of surface tiles in CLM5 at the gridcell containing the SGP site.

Surface Type	**Percent of Total Grid Area (%)**
C3 crop	48.74
C3 grass	25.56
C4 grass	22.17
C3 irrigated crop	2.26
Broadleaf deciduous temperate tree	0.66
Bare ground	0.32
Needleleaf evergreen temperate tree	0.15
Urban	0.15

As in H22, SCAM simulations follow a hindcast approach: the model is run for two days, discarding the first day for model spin-up and using the second day for analysis. Unlike in H22 however, we do not create a continuous time series of summer (June-August) days in 2015. Instead, we select days that have been simulated by WRF-LES as part of an extension to Simon et al. (2021), which are documented in Simon et al. (2022).

Simon et al. (2021) simulated three shallow convection days at the ARM SGP site using WRF-LES (Skamarock et al., 2008). On each day, a 100x100 km domain was forced by either homogeneous or heterogeneous surface conditions. In the heterogeneous case, an offline land

model (HydroBlocks; Chaney et al., 2016) was used to supply prescribed surface fluxes, temperature, albedo, and momentum drag coefficients to each atmospheric column. The homogeneous case forces every column by the grid-mean values of these terms instead. Since those initial experiments were conducted, the work has expanded to include 92 shallow convection days (Simon et al., 2022). The increased temporal sampling necessitated a degradation in horizontal resolution to 250x250 m (compared to 100 m in the original set of three days), and covers a slightly larger domain of 130 x 130 km.

In this study, we focus on the warm season when land-atmosphere interactions in the central United States are strongest. We therefore simulate a subset of all available WRF-LES days, covering 60 days between May and September in 2015-2018. All LES-based analysis is limited to this subset of 60 days as well. We search for a similar atmospheric signal in SCAM as was seen in WRF-LES: increased turbulence relative to HOM and increases in $\overline{\theta_l'^2}$,and $\overline{q_t'^2}$. We are not attempting to align the control cases between WRF-LES and SCAM in this study. There are a number of reasons to anticipate the two may not agree regardless, including differences in the land models providing the surface forcing and the formation of organized convection and rainfall in LES, which is difficult to capture in SCAM. Instead, we compare the relative atmospheric change between HET and HOM cases across models. Two sets of SCAM sensitivity experiments are also conducted to determine the impacts of stronger surface heterogeneity and a continuous convection scheme. These are introduced in Section 3.3, but are included in Table 2 as a reference for all SCAM experiments conducted.

Table 2: Single-column CESM2 experiments and descriptions.

SCAM Experiment	Description
HOM	Following the original equations laid out in André et al. (1978) in Eq. 1-3, this is roughly analogous to the default behavior of CLUBB in CESM2.
HET	Surface variances of temperature and moisture are modified to include a heterogeneous term, as in Eq. 4-6.
HET_{α}	As in HET, but with the SGS surface variances in Eq. 4-6 scaled to match the lowest model level daily maximum variance in WRF-LES.
HOM_{noDC}	As in HOM, but with the default deep convection scheme turned off so that CLUBB is responsible for both shallow and deep convection.
HET_{noDC}	As in HOM_{noDC}, but with the CLUBB surface variances modified to include the effects of SGS heterogeneity as in HET.
HET_{α_noDC}	As in HET_{noDC}, but with the magnitude of SGS surface variances scaled to match the LES experiments as in HET_{α}.

3 Results

3.1 Atmospheric response to surface heterogeneity in SCAM

The diurnal evolution of several CLUBB variables in HOM are shown in the left column of Figure 1. Each variable has been interpolated from the model's raw hybrid coordinates to

constant pressure levels from 970-200 hPa with a 10 hPa resolution. The 60-day record simulated by SCAM is then averaged to define composite HOM and HET cases.

As the surface warms, HOM $\overline{\theta_l'^2}$ peaks at 0.1 K^2 in the lowest model level at 14 local time (LT) (*Fig. 1a*). Variances greater than 0.05 K^2 are confined to the lowest model levels, but a weaker secondary peak occurs near the top of the PBL. The maximum of $\overline{q_t'^2}$ occurs closer to the top of the PBL as well, at 820 hPa (*Fig. 1c*). Both peaks along the upper boundary of the PBL are driven by entrainment between the near-surface layer and free troposphere; near that boundary, as warmer/drier air mixes with cooler/wetter air, the covariance between the two fields becomes negative (*Fig. 1e*). As the co(variances) grow during the day, PBL turbulence increases as well due to an increase in the turbulent heat flux ($\overline{w'\theta_l'}$) (*Fig. 1g,i*). Note that CLUBB represents atmospheric turbulence only through $\overline{w'^2}$ which evolves following Eq. 7 (adapted from Larson (2017)):

$$\frac{\partial \overline{w'^2}}{\partial t} = \overline{w}\frac{\partial \overline{w'^2}}{\partial z} - \frac{1}{\rho_s}\frac{\partial \rho_s \overline{w'^3}}{\partial z} - 2\overline{w'^2}\frac{\partial \overline{w}}{\partial z} + \frac{2g}{\theta_{vs}}\overline{w'\theta_v'} - \frac{2}{\rho_s}\overline{w'\frac{\partial p'}{\partial z}} - \epsilon_{ww} \quad (7)$$

Where ρ_s is the basic state air density, θ_{vs} is the dry, base-state virtual potential temperature, g is the gravitational acceleration, and ϵ_{ww} is the turbulent dissipation.

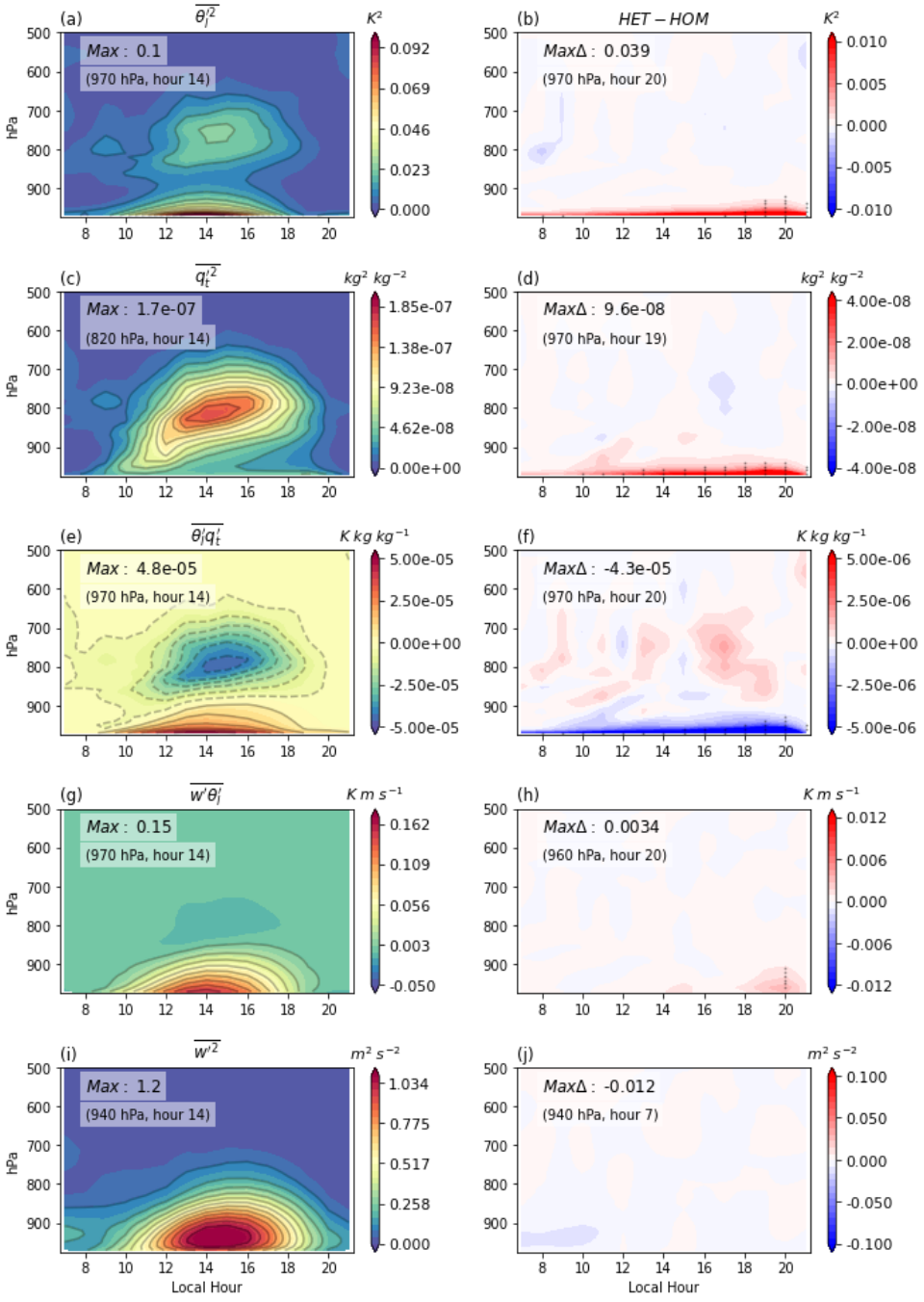

Figure 1: *Time-height plots of (left) HOM temperature variance (a), moisture variance (c), their covariance (e), eddy-flux of temperature (g), and vertical velocity variance (i), averaged over all 60 days; and (right) HET-HOM for each variable. Stippling indicates significant differences at the 95% confidence level based on the standard error (defined as the standard deviation normalized by the square root of the number of samples) at each hour/level. Inset text provides the timing/height of the maximum value within the range of levels shown.*

When SGS heterogeneity is included in the calculation of the near-surface moments, $\overline{\theta_l'^2}$ and $\overline{q_t'^2}$ increase relative to *HOM* (*Fig. 1b,d*). The increase, however, is statistically significant only

below 920 hPa (stippling in *Fig. 1* denotes significance at the 95% confidence level, determined by the standard error). Significant increases in $\overline{\theta_l'^2}$ are also limited temporally, from ~17-21 LT and maximizing at 20 LT. The $\overline{q_t'^2}$ increases in HET are statistically significant for a more extended period of 10 LT onwards, though again the change is largest in the evening (9.6e-8 kg^2/kg^2 at 19 LT). The covariance $\overline{\theta_l' q_t'}$ decreases in HET at a magnitude that is statistically significant for most hours as well, with a maximum change of -4.3e-5 K kg/kg (*Fig. 1f*). During the evening hours, that decrease is enough to reverse the sign of $\overline{\theta_l' q_t'}$ such that it becomes negative at the lowest level (i.e., positive temperature anomalies are associated with negative moisture anomalies) and limits the turbulent moisture flux (not shown). Ultimately then, the addition of SGS heterogeneity does not act to increase the absolute peak of temperature/humidity (co)variances, which occurs in the afternoon. Instead, HET enhances these values in the late evening. At the timing of peak differences, HOM $\overline{\theta_l'^2}$ has dropped to 0.01 K^2, $\overline{q_t'^2}$ to 4.8e-8 kg^2/kg^2 , and $\overline{\theta_l' q_t'}$ to 1.0e-5 K kg/kg, all well below their diurnal maximum.

To better understand how and why the inclusion of SGS heterogeneity increases near-surface $\overline{\theta_l'^2}$ and $\overline{q_t'^2}$ in the evening and reverses the sign of $\overline{\theta_l' q_t'}$, we evaluate the tile-level temperature and moisture values in CLM5. Their departures from the gridcell-mean are all that differentiate the HET and HOM calculations in Eq. 4-6. Figure 2 shows the diurnal cycle of the grid-mean variance in temperature (Fig. 2a) and moisture (Fig. 2b), again averaged over all 60-days that were simulated. That is, the top row of Figure 2 shows the second term in Eq. 4-6 that represents the addition of heterogeneity. As expected, the timing of the largest variances align with the hours where HET differences in Figure 1 peak and are statistically significant.

Note that the diurnal cycle of these patch-level variances differ from the typical diurnal cycle of near-surface temperature and humidity, and from the timing of maximum variance in HOM. Although grid-mean 2-m temperature typically peaks in the late afternoon and its variance peaks slightly earlier than that in the control case, the SGS surface variance simulated by CLM5 does not peak until ~20 LT. The evening maximum here is primarily the result of more rapid cooling over the C3 rain-fed crop patch, covering almost half of the gridcell, compared to a slower cooling rate over C4 and C3 grasses, which combined cover just over 47% of the grid area (dark blue dashed line vs. dashed cyan and solid green lines respectively, *Fig. 2c*). These differential cooling rates occur while the mean high-level cloud fraction is greater than 50% during the evening, with a longwave cloud forcing of ~3.5 W/m^2 (thus, this is not a clear-sky signal). The moisture variance in CLM5 also peaks in the evening but increases more steadily throughout the day as the humidity over C3 grasses tends to remain lower than the grid mean while the moisture over crops remains higher, with the differences between those two tiles peaking between 18-20 LT. That largely results from a higher transpiration rate in rain-fed crops compared to grasses, which creates a more humid and cooler near-surface over C3 crops and drives a negative covariance between temperature and moisture at the patch-level. In the evening, when the HOM covariance in CLUBB has dropped to a small but still positive value, the large negative covariance in HET reverses the overall signal at the lowest model level.

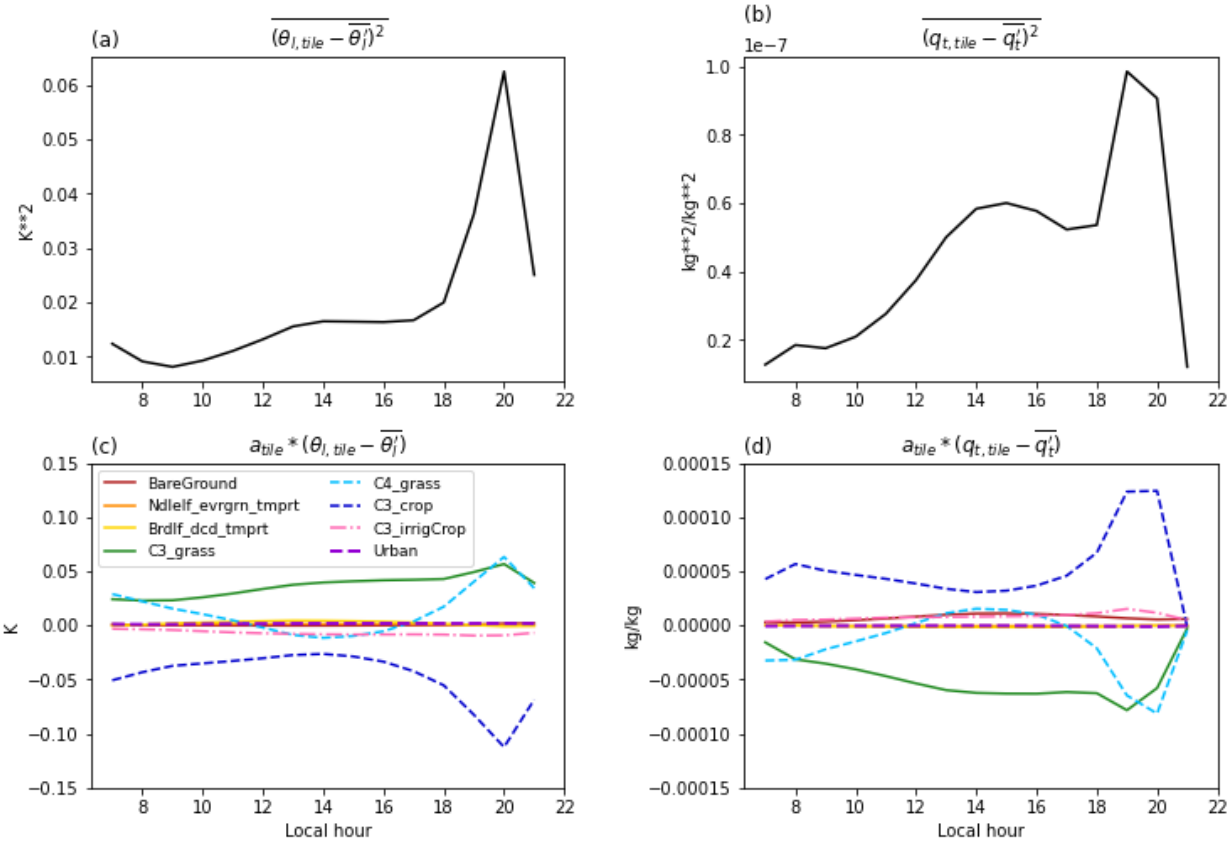

Figure 2*: Mean diurnal cycles of variance across surface patch (a) temperature and (b) humidity. (c, d) The grid area-weighted difference in temperature and humidity for each patch relative to the gridcell mean value, which is used to compute the grid mean variances.*

Although the near-surface higher-order moments evolve as expected in *HET*, the impacts on atmospheric turbulence are limited. Based on the findings of Simon et al. (2021), SGS surface heterogeneity is expected to increase PBL turbulence. Yet there are no statistically significant $\overline{w'^2}$ increases in CLUBB (*Fig. 1j*) despite small increases in $\overline{w'\theta_l'}$ (*Fig. 1h*). This is likely a result of WRF-LES explicitly representing the phenomena that generate increases in turbulent kinetic energy (TKE); CLUBB does not resolve those actual processes and instead relies on parameterizations of their source terms. That parameterization, however, allows us to better understand how changing the near-surface (co)variances in temperature and/or moisture could drive an increase in turbulence.

Mathematically, an increase in atmospheric turbulence is achievable in CLUBB through an increase in $\overline{\theta_l'^2}$. The time-evolving vertical velocity variance (Eq. 7) depends in part on a buoyancy production term, $\frac{2g}{\theta_{vs}}\overline{w'\theta_v'}$, and thus the grid-mean eddy flux of virtual potential temperature. This turbulent temperature flux is in turn dependent on the temperature variance through its inclusion in the buoyancy production term of Eq. 3.2 in Larson (2017), $\frac{g}{\theta_{vs}}\overline{\theta_l'\theta_v'}$, where the covariance of liquid water and virtual potential temperature is tightly correlated to the variance of liquid water potential temperature alone. Computing each term of the $\overline{w'^2}$ budget

following Eq. 7 indicates that the *HET* experiment drives a slight increase in the near-surface buoyancy production term due to the enhanced $\overline{w'\theta_l'}$, (solid teal line in Fig. 3), but the increase is too small to drive a statistically significant response in the total vertical velocity variance.

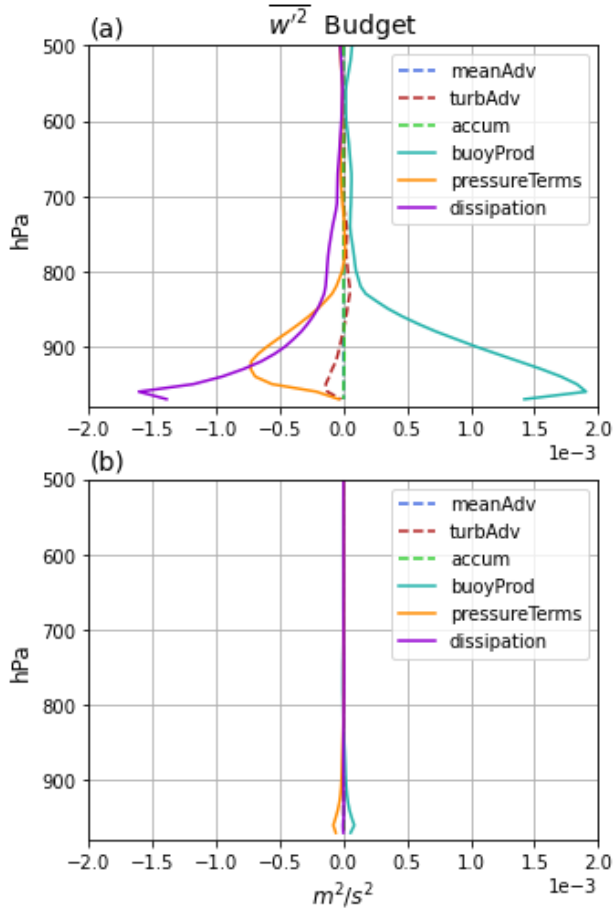

Figure 3*: Mean budget terms of* $\overline{w'^2}$ *as in Eq. 7 for (a) HOM and (b) HET-HOM. Profiles are averaged from 17-21 LT, the hours at which the changes in* $\overline{\theta_l'^2}$ *are statistically significant.*

3.2 Atmospheric response to surface heterogeneity in WRF-LES

The above changes in higher-order moments and turbulence in SCAM can be directly compared with WRF-LES experiments averaged over the same set of 60 days and driven by higher-resolution LASSO-VARANAL forcing (*Fig. 4*). Again, we emphasize that we do not expect nor find agreement between WRF-LES and SCAM *HOM* cases. The two in fact differ substantially, with $\overline{\theta_l'^2}$ reaching a maximum aloft in LES (1.4 K^2 at 662 hPa) rather than near the surface as in CLUBB (*Fig. 4a*). The values of $\overline{q_t'^2}$ are slightly more similar between models in where they peak (~790 hPa in LES vs. 820 hPa in SCAM), though the maximum is more than four times larger in LES (*Fig. 4c*). The lowest level variances themselves can differ markedly between models, though again this is not unexpected; potential sources for that disagreement are explored further in Section 3.3. Atmospheric turbulence in WRF-LES *HOM* is more than twice as large as in SCAM as well, but the peak again occurs near the surface and during the mid-afternoon (*Fig.*

4e). Note that in WRF-LES, TKE is computed as half the sum of the meridional, zonal, and vertical velocity variances for consistency with Simon et al. (2021). In both this and SCAM, however, the calculation reflects how the different atmospheric models generate turbulence.

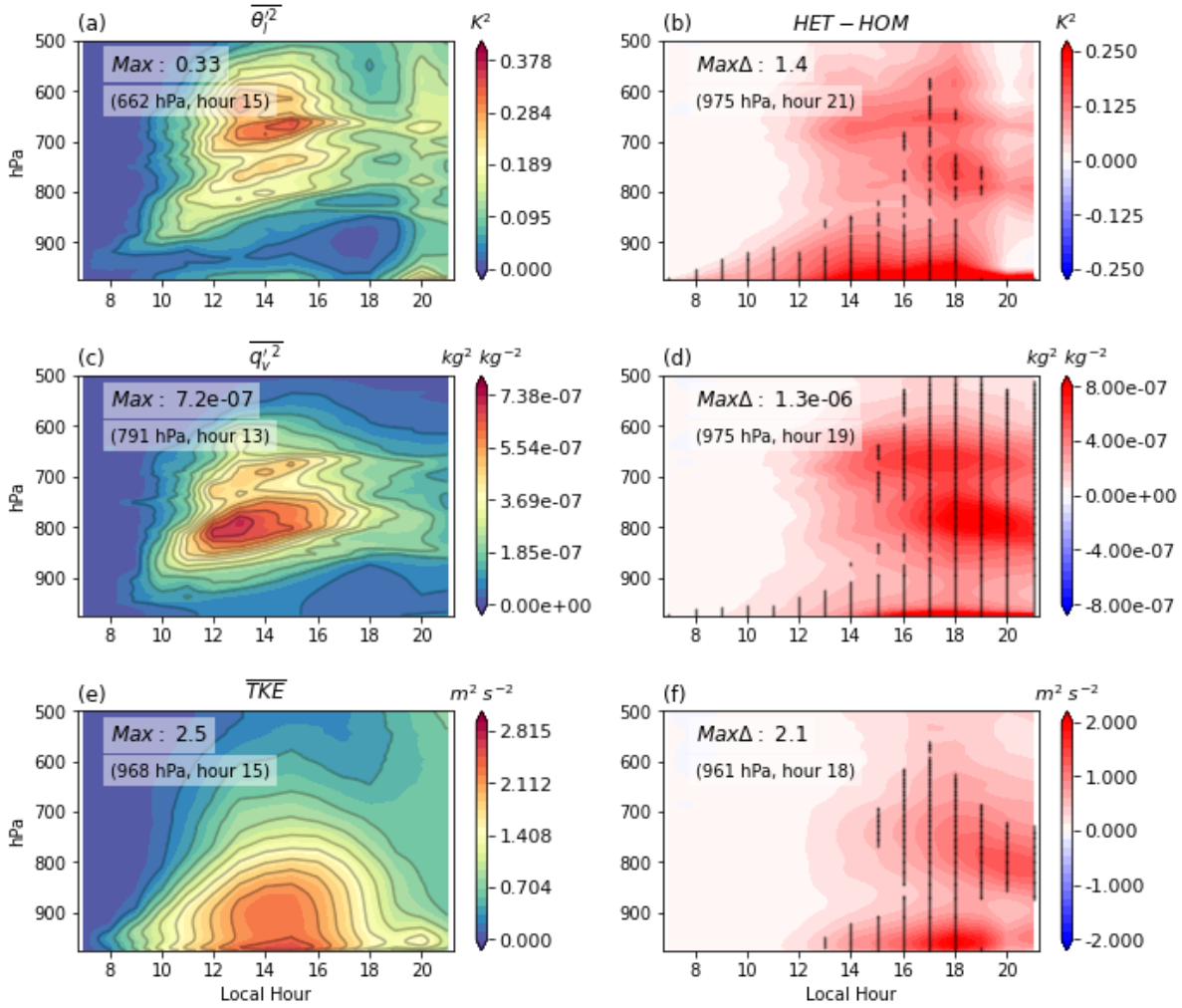

Figure 4*: As in Figure 1, but for the WRF-LES experiments*

In WRF-LES *HET* cases, we find the expected increase in near-surface $\overline{\theta_l'^2}$ and $\overline{q_t'^2}$ due to spatially varying fluxes (*Fig. 4b,d*). The largest changes in magnitude are again located near the surface and occur in the late evening, suggesting that the SCAM *HET* case is capturing at least part of the heterogeneity signal reasonably well. Unlike SCAM, however, significant increases in WRF-LES variances extend well beyond the lowest model levels (up to ~575 hPa at 17 LT for $\overline{\theta_l'^2}$, and beyond that for $\overline{q_t'^2}$). But this vertical extension appears to be somewhat disconnected from the surface signal, as the magnitude of $\overline{\theta_l'^2}$ and $\overline{q_t'^2}$ changes are not continuous. Thus the increases that occur at the surface and aloft may result from different physical mechanisms. The increased magnitude and extent of these higher-order moments coincides with TKE increases of up to 2.1 m^2/s^2 during the evening, but again there appear to be two centroids to the *HET* response, one near the surface and one near 800 hPa (*Fig. 4f*).

Assessing individual days in the record rather than the 60-day mean confirms that the elevated *HET* increases in WRF-LES are typically separate from the near-surface signal. We hypothesize that this is due to the explicit representation of mesoscale secondary circulations that arise between warm/dry and cool/wet patches. Those circulations then organize convection and rainfall, as illustrated below for the main day assessed by Simon et al. (2021) (*Fig. 5*). The elevated increases in $\overline{\theta_l'^2}$, $\overline{q_t'^2}$, and TKE align with the formation and organization of shallow convection around 13-14 LT, and are not directly tied to the surface variance of temperature or moisture. This is in agreement with the findings of Simon et al. (2022), who confirm that the largest changes in TKE and liquid water path occur as a result of mesoscale secondary circulations ($\mathcal{O}$(10 km) or greater) in an assessment of all 92 WRF-LES cases. CLUBB, which is described by simple continuous PDFs of temperature, moisture, and vertical velocity, is not designed to capture the turbulence characteristics of overturning circulations that span the gridcell. It is therefore likely that SCAM experiments will be unable to match the vertical structure of the WRF-LES *HET* response without additional development efforts to properly capture these structures.

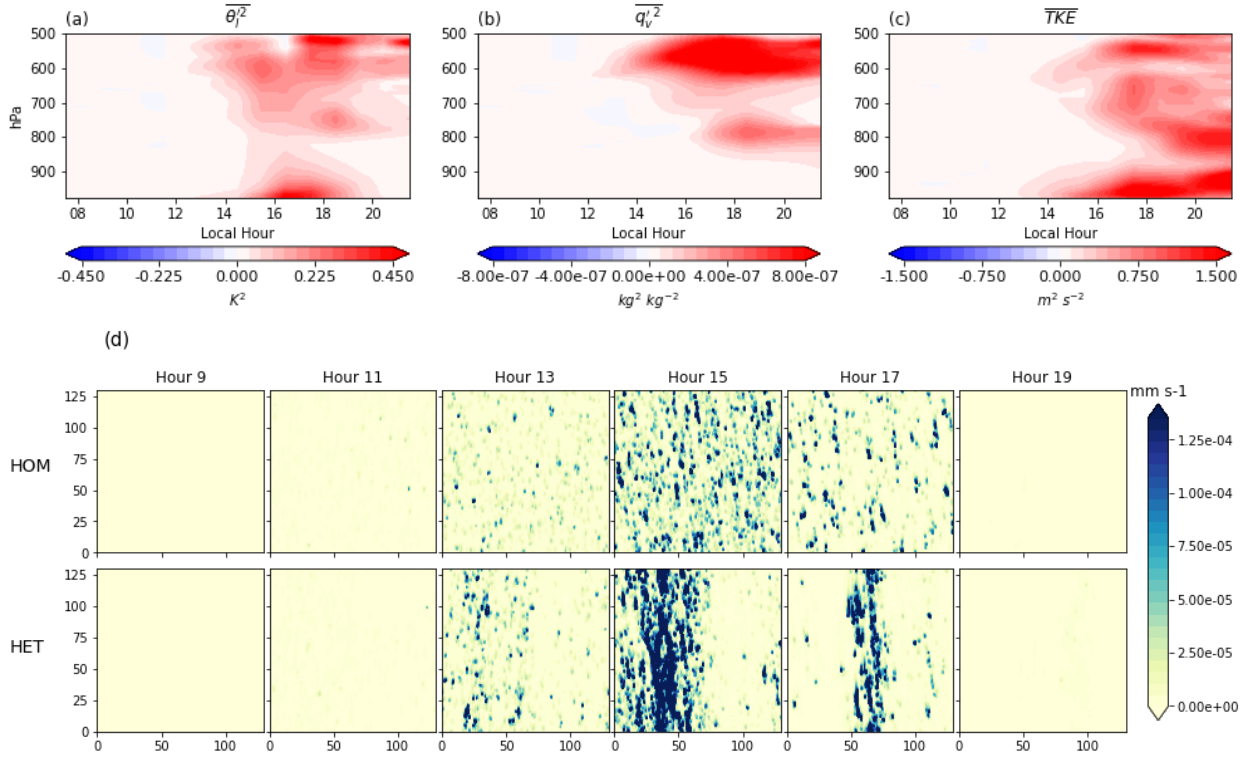

Figure 5*: A single-day case study (9/24/2017) of WRF-LES HET-HOM (a) moisture variance, (b) temperature variance, and (c) TKE; (d) hourly mean snapshots of rainfall in HOM (top) and HET (bottom).*

There are, however, additional reasons why the atmospheric response to SGS heterogeneity might be expected to differ between SCAM and WRF-LES. From a land surface perspective, the subgrid heterogeneity is computed by two different land models in these experiments. CLM5 provides the surface information to SCAM, but high resolution HydroBlocks simulations are

used to provide surface boundary conditions to WRF-LES. The latter ingests observed precipitation at a 4 km resolution so that the impact of SGS meteorology is reasonably captured across the entire 130x130 km^2 domain. This is especially critical in the central United States, where scattered thunderstorms and mesoscale systems are a common feature of the summer climatology, but cover less than a full GCM gridcell (i.e., ≥1˚). Their impact on surface temperature and moisture variance is thus explicitly included in HydroBlocks but not in CLM5, which contributes to differences in the HOM cases as well.

From an atmospheric perspective there are potentially critical model differences as well, aside from the fact that CLUBB does not represent large-scale secondary circulations. WRF-LES includes an explicit representation of convective processes that enables shallow convection to transition smoothly into resolved deep convection. While SCAM contains its own deep convection parameterization (G. Zhang and MCFarlane, 1995; Neale et al., 2008), it is separated from the moist turbulence processes in CLUBB. There is therefore a conceptual jump between CLUBB-based shallow convection and deep convection, where the presence of SGS heterogeneity is being implicitly conveyed to the deeper atmosphere. A more continuous representation of the transition between shallow and deep convection could be important for realizing the impacts of surface heterogeneity on the overlying atmosphere. This is particularly of interest given the elevated HET signal that occurs in WRF-LES but is absent in SCAM.

3.3 SCAM Sensitivity Experiments

Though some model limitations outlined above require additional parameterization development and/or significant model calibration, appropriate testing through sensitivity experiments could reveal shortcomings in the existing CLUBB configuration. Two additional sets of SCAM experiments are thus conducted to explore the potential impacts of SGS meteorology and of a more continuous convection scheme, discussed in turn below.

Scattered sub-grid precipitation is expected to increase SGS temperature and moisture variances within CLM5, as only a fraction of the domain would experience soil moisture increases and surface cooling. We approximate that impact by scaling the heterogeneous terms in Eq. 4-6 so that the grid-mean fluxes and states that define the HOM moments remain the same, but the difference between surface tiles that produce those values is amplified. The control case (HOM) is therefore unchanged, but we conduct a new set of heterogeneous surface experiments, HET_α:

$$\overline{\theta_l'^2}_{HET_\alpha} = \overline{\theta_l'^2}_{HOM} + \alpha_\theta * \overline{\left(\theta_{l,tile} - \bar{\theta}_l\right)^2} \tag{8}$$

$$\overline{q_t'^2}_{HET_\alpha} = \overline{q_t'^2}_{HOM} + \alpha_q * \overline{\left(q_{t,tile} - \bar{q}_t\right)^2} \tag{9}$$

$$\overline{\theta_l' q_t'}_{HET_\alpha} = \overline{\theta_l' q_t'}_{HOM} + \sqrt{\alpha_\theta} * \sqrt{\alpha_q} * \overline{(\theta_{l,tile} - \bar{\theta}_l)(q_{t,tile} - \bar{q}_t)} \tag{10}$$

The magnitude of the multipliers α_θ and α_q is allowed to vary according to day and is determined by comparing the original HET cases with the equivalent WRF-LES experiments. For each day, the maximum $\overline{\theta_l'^2}$ and $\overline{q_t'^2}$ at the lowest model level in WRF-LES is compared to

449 the maximum spatial variance at the lowest model level in the SCAM HET case. The values of
450 α_θ and α_q are the ratios of these maxima, designed to ensure nearly equal low-level forcing in
451 both model frameworks. On average, this requires values of 51.1 for α_θ and 23.9 for α_q. We also
452 conduct a high-end and low-end experiment, where both α_θ and α_q are set to 100 (HET_{100}) or 10
453 (HET_{10}) for all 60 days. Yet even the HET_α experiment should be considered an upper bound on
454 the magnitude of heterogeneity one could expect to represent in SCAM. The lowest level in
455 WRF-LES is closer to the surface than in SCAM (~15 m vs. 30 m) and has a much shorter
456 timestep (0.5 seconds vs. a 5 minute CLUBB timestep); thus even the HOM column-maximum
457 variances estimated by CLUBB can be an order of magnitude lower than in WRF-LES.
458 Nonetheless, the approach provides an initial indication of how sensitive CAM6 may be to
459 surface heterogeneity if LES-type SGS meteorology were represented.
460
461 Comparing the atmospheric response in HET_α to HET, we find that the vertical extent of
462 statistically significant differences in higher order moments increases and spans most of the day
463 (*Fig. 6* vs. the right column of *Fig. 1*). At 20 LT, heterogeneity-induced increases in $\overline{\theta_l'^2}$ peak at
464 0.37 K^2 at the lowest model level, but statistically significant increases extend to 900 hPa (*Fig.*
465 *6a*). The largest change in $\overline{q_t'^2}$ occurs at 8 LT, but the largest statistically significant change
466 occurs at 16 LT, with small but significant changes extending to 850 hPa at 21 LT (*Fig. 6b*). But
467 regardless of how large the surface heterogeneity forcing is, increases in (co)variances are
468 confined to pressure levels below 800 hPa and are topped by changes of the opposite sign. Such
469 a dipole pattern in the heterogeneity signal is not observed in WRF-LES, where the organization
470 of convection and rainfall (again, a phenomenon CLUBB does not capture) likely increases $\overline{\theta_l'^2}$
471 and $\overline{q_t'^2}$ instead.

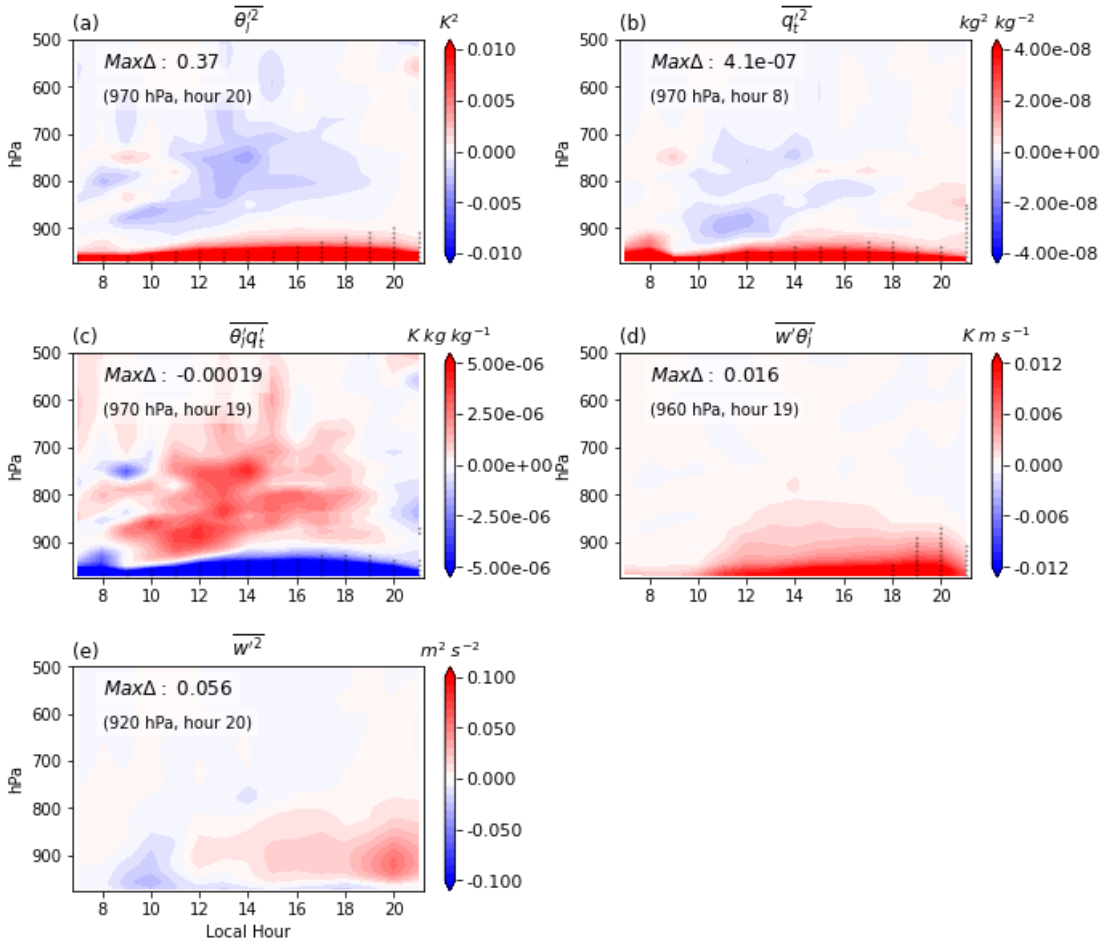

Figure 6*: As in the right column of Figure 1, but with differences taken between* HET_α and HOM *cases.*

Turbulence increases in HET_α are stronger than those in the original HET case, but are not statistically significant (*Fig. 6e*), despite significant increases in $\overline{w'\theta_l'}$ (*Fig. 6d*). These changes are, however, qualitatively similar to the WRF-LES response. As before, we assess the $\overline{w'^2}$ budget to assess the mechanism behind the afternoon/evening increase (*Fig. 7*). The HET_{10} and HET_{100} cases are included for additional context. Compared to Figure 3b, the HET-scaling experiments all induce a stronger and deeper atmospheric response (*Fig. 7*). The increase in near-surface $\overline{\theta_l'^2}$ drives an increase in the buoyancy production term and a compensating decrease in the pressure and dissipation terms. The magnitude and vertical extent of that change scales with the magnitude of the surface heterogeneity, with HET_{100} able to communicate these changes to a depth of ~800 hPa compared to 850-825 hPa in HET_α and HET_{10}. HET_{100} is also the only case to produce statistically significant increases in evening turbulence (not shown). It is therefore possible to increase turbulence in SCAM without an explicit representation of mesoscale secondary circulations, but it requires a significant increase in the magnitude of surface heterogeneity relative to what CLM5 originally predicted.

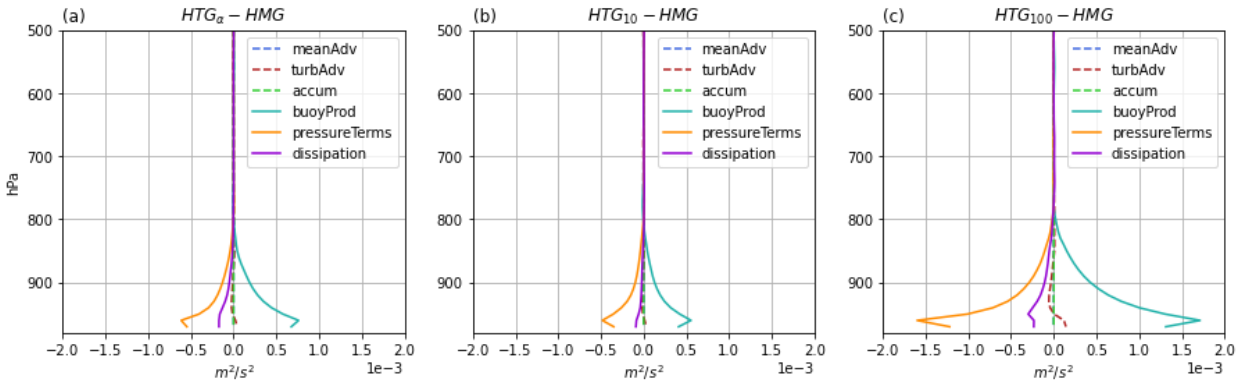

***Figure 7**: As in Figure 3b, but for the three HET-scaling experiments introduced above. Averages are again taken from 17-21 LT.*

The HET_{100} case is also the only SCAM experiment to produce a noticeable precipitation change (*Fig. 8*), and is the only one that comes close to producing a similar distribution of hourly mean rainfall compared with WRF-LES. The SCAM HOM, HET, and HET_α cases are all nearly identical in their distributions, with a longer tail of near-zero rain rates. These SCAM cases also have a single peak in rain rates (~0.1 mm/hr), though both the WRF-LES HET case and the observed rain rates from the LASSO VARANAL dataset (gray and black lines in *Fig. 8*) are bimodal. HET_{100} produces an appreciable second peak in precipitation and significantly reduces the frequency of near-zero rain rates (pink line in *Fig. 8*). Though the overall shape of the distributions are similar between the WRF-LES HET and SCAM HET_{100} cases, the discrepancy in height between the two suggests that SCAM continues to rain more frequently than WRF-LES.

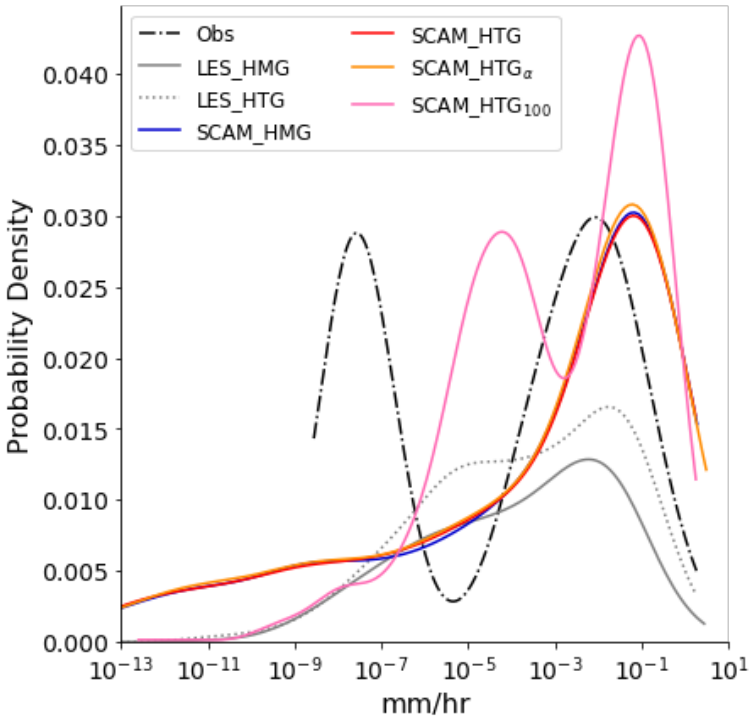

Fig 8*: PDF of hourly mean rain rates in the LASSO VARANAL data set (black dash-dot line), WRF-LES (gray lines), and SCAM (colored lines), compiled over all 60 days from 7-23 LT. Hours used in constructing the PDF are conditioned on grid-mean rain rates being >0, such that the number of samples varies across simulations if one contains more frequent rainfall.*

Although HET_{100} produces a more sizable turbulence and precipitation response, the magnitude of the multiplier is likely unrealistic. Very few days in WRF-LES suggest α_θ or α_q values that large, even given the disparity in vertical and temporal resolution between the two models. Seven days required $\alpha_\theta \geq 100$, and four days required $\alpha_q \geq 100$. Thus, while HET_{100} is useful for assessing if any modification of CLUBB's surface boundary conditions can drive a strong atmospheric response, this is not a reasonable option for achieving agreement between WRF-LES and SCAM.

These scaling experiments suggest that the disagreement in WRF-LES and SCAM responses to SGS surface heterogeneity is not solely the result of different surface (co)variance magnitudes. We thus explore a second possibility, that the increase in higher-order moments used as boundary conditions for CLUBB is not being felt by the deep convection scheme in SCAM, thereby limiting the atmospheric response. In this sensitivity test, we define a new set of homogeneous and heterogeneous SCAM cases wherein the deep convection scheme is switched off; this ensures that CLUBB handles all convection regardless of its characterization as shallow or deep (these cases are denoted as HOM_{noDC} and HET_{noDC}, respectively). We also test the hypothesis that both factors (continuous convection as well as larger surface variances) could interact, computing a multiplier for the heterogeneous terms as in HET_α, but based on the ratio of HET_{noDC} and WRF-LES daily maxima; this case will be referred to as HET_{α_noDC}.

Eliminating the separation between shallow and deep convection schemes in SCAM is not sufficient to produce a $\overline{\theta_l'^2}$ and $\overline{q_t'^2}$ increase that is consistent with WRF-LES (*Fig. 9a,c*). In general, the signal in HET_{noDC} is similar to HET – increases in variances are limited vertically, and temporally for $\overline{\theta_l'^2}$. Turbulence increases slightly, but the change is still not statistically significant (*Fig. 9i*).

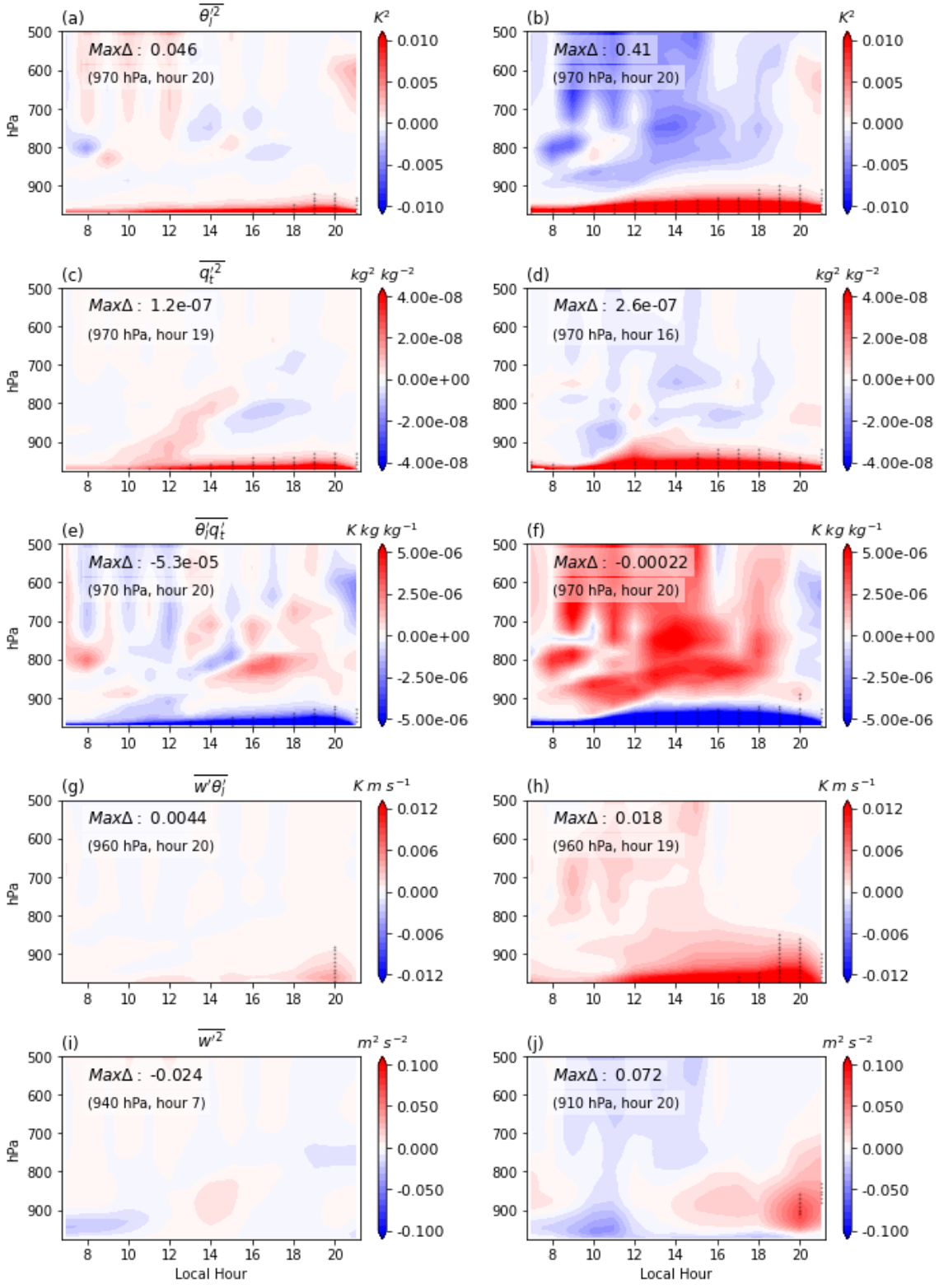

***Figure 9**: As in Figure 6, but for cases without a separate deep convection scheme. (Left) HET_{noDC}- HOM_{noDC}; (right) HET_{α_noDC}- HOM_{noDC}*

Increasing the magnitude of surface heterogeneity in HET_{α_noDC} increases the vertical extent of significant increases in $\overline{\theta_l'^2}$ and $\overline{q_t'^2}$ to 900 hPa and 920 hPa, respectively, and extends the number of hours at which changes are significant (*Fig. 9b,d*). Those increases are again accompanied by a broader low troposphere signal of the opposite sign, but without representing secondary circulations and the resulting organization of convection, elevated increases are a difficult WRF-LES feature for SCAM to emulate. Yet HET_{α_noDC} achieves an increase in evening turbulence that is statistically significant and stretches to 830 hPa (*Fig. 9j*).

Combined, these sensitivity experiments have explored two potential hypotheses for why WRF-LES and SCAM differ in their response to SGS surface heterogeneity, but neither sufficiently explains the current disparity. A representation of SGS meteorology combined with a more continuous convection representation in SCAM both hold promise for improving model agreement, but additional factors likely play a critical role. It is beyond the scope of the current study to investigate all of these potential drivers, but a more explicit representation of mesoscale secondary circulations is likely a necessity in future development efforts based on the results of Simon et al. (2022) and the current SCAM shortcomings shown here.

4 Discussion and Conclusions

In this study, we explored a new CESM2 coupling strategy designed to capture the impacts of SGS surface heterogeneity on the atmosphere. The approach links information on the distribution of temperature and moisture across surface tiles in CLM5 with CLUBB's boundary conditions in CAM6. To investigate the impact of this new addition, a series of SCAM experiments were conducted at the ARM SGP site on 60 warm season shallow convection days, which were compared to a similar existing set of WRF-LES simulations (Simon et al., 2021, 2022). Although LES output should not be conflated with observations (there is no guarantee that the WRF-LES sensitivity to heterogeneity is accurate), the experiments offer a unique opportunity to explicitly isolate the role of surface heterogeneity each day and its impact on higher order, difficult to observe variables.

In WRF-LES, SGS heterogeneity increases the grid-mean variance of temperature and moisture, with statistically significant differences relative to HOM that grow in the vertical during the afternoon to depths of nearly 500 hPa. There are two unique centroids within this atmospheric response - one near the surface, and another more elevated one that becomes apparent in the late afternoon. The latter is hypothesized to result from mesoscale secondary circulations initiated by variability in surface sensible and latent heat fluxes in the HET case. These structures increase afternoon/evening TKE and help organize convection and precipitation (Simon et al., 2022).

The SCAM parameterization produces a markedly weaker atmospheric response to heterogeneity. Increases in HET temperature and moisture variances are smaller than those in WRF-LES, and are more constrained vertically and temporally. This results in no discernable increase in turbulence. We attempt to diagnose the reason for such a limited atmospheric response through a series of additional experiments that isolate important model differences between WRF-LES and SCAM.

The WRF-LES experiments are forced at the surface by a high-resolution land model that captures the impacts of SGS meteorology on soil moisture and temperature. CLM5 does not yet have a similar capability, though recent developments do enable the downscaling of incoming radiation, temperature, and precipitation due to variations in topography (Swenson et al., 2019). The SGP site is fairly uniform in elevation however, such that this downscaling has little to no impact on the computed variances of temperature and humidity. Instead, we approximate the effect of scattered storms by applying a scaling factor that artificially increases the magnitude of heterogeneity within the gridcell (HET_{α}, HET_{10}, and HET_{100}). Though this approach does slightly increase the vertical and temporal extent of significant differences in the (co)variances of temperature and moisture, it is still unable to generate a statistically significant heterogeneous signal similar to that in WRF-LES. Only in the HET_{100} case are differences in $\overline{w'^2}$ statistically significant, as the surface boundary conditions used in CLUBB are large enough to drive a large and deep increase in buoyancy production through enhanced turbulent fluxes of virtual potential temperature. This is also the only experiment capable of producing altered precipitation statistics that align with some aspects of WRF-LES (e.g., bimodal distributions with limited near-zero rain rates). Despite these encouraging signs, the magnitude of the scaling applied is likely unrealistic.

Another important difference between the SCAM and LES models is in their representation of convection. The high vertical, horizontal, and temporal resolutions used in LES explicitly resolves the continuous transition between shallow and deep convection without an artificial switch between convective parameterizations; the same cannot be said for SCAM. We thus experiment with turning off the deep convection scheme and allowing CLUBB to handle all convection that develops in the grid, even if it grows to deeper levels. While the HET_{noDC} experiment indicates a small but not significant increase in turbulence, $\overline{\theta_l'^2}$, $\overline{q_t'^2}$, and $\overline{\theta_l' q_t'}$ continue to respond only near the surface. Combining our two sensitivity experiments by applying a multiplier to the cases without a separate deep convection scheme, HET_{α_noDC} comes close to qualitatively agreeing with WRF-LES, though heterogeneity-induced changes continue to be vertically limited.

The above sensitivity experiments are not sufficient to definitively answer the question of what causes the difference in WRF-LES and SCAM responses to SGS heterogeneity, but they do highlight the complex nature of the problem. Critically, the current SCAM parameterization lacks the ability to explicitly represent secondary circulations, which Simon et al. (2022) suggest are critical to the atmospheric response present in these WRF-LES experiments. In other observational and LES experiments as well, the atmospheric differences that arise over heterogeneous surfaces stem from these mesoscale secondary circulations that transport heat and moisture between parts of the domain (Cioni & Hohenegger, 2018; Avissar & Schmidt, 1998; Doran et al., 1995; Ookouchi et al., 1984). Such circulations are currently outside the scope of what CLUBB is designed to capture in its statistical representation of SGS heterogeneity, and the parameterization implemented here was not intended to add that phenomenon to the model. Instead, the intent was to capture the impact these circulations have on surface variances and back out a response in CLUBB through that pathway alone. It is likely, however, that further development efforts will require a more thorough representation of secondary circulations to create a more realistic atmospheric response to surface heterogeneity. Ongoing work to represent not only eddy diffusivity (as in CLUBB) but also mass fluxes within climate models thus holds particular promise for its ability to mix surface states and fluxes more thoroughly in the vertical.

633 Future work should focus on pathways to communicate the impacts of surface heterogeneity to
634 the atmosphere not just through surface boundary conditions but in ways that can influence the
635 vertical and horizontal transport of energy and moisture in a spatially organized manner.

636

637 **Acknowledgments**

638 Funding for this work was provided by NOAA grants NA19OAR4310241 and

639 NA19OAR4310242. Additional support for MDF was provided through NSF award 1755088.

640

641 **Open Research**

642 Simulations are run with a modified version of CESM2 that enables the calculation of CLUBB's

643 surface boundary conditions in the land model; the model source code including thse

644 modifications, SCAM model output, and analysis scripts are available at Fowler et al. (2022).

645 The WRF-LES model output is currently publicly available from

646 http://hydrology.cee.duke.edu/CLASP/LES/diags2/.

647

648 **References**

649 André, J. C., de Moor, G., Lacarrere, P., Therry, G., & du Vachat, R. (1978). Modeling the 24-
650 hour evolution of the mean and turbulent structures of the planetary boundary layer. *Journal of*
651 *the Atmospheric Sciences*, *35*, 1861–1883. https://doi.org/https://doi.org/10.1175/1520-
652 0469(1978)035<1861:MTHEOT>2.0.CO;2

653 Avissar, R., & Liu, Y. (1996). Three-dimensional numerical study of shallow convective clouds
654 and precipitation induced by land surface forcing. *Journal of Geophysical Research:*
655 *Atmospheres*, *101*(D3), 7499–7518. https://doi.org/https://doi.org/10.1029/95JD03031

656 Avissar, R., & Pielke, R. (1989). A parameterization of heterogeneous land surfaces for
657 atmospheric numerical models and its impact on regional meteorology. *Monthly Weather*
658 *Review*, *117*, 2113–2136. https://doi.org/https://doi.org/10.1175/1520-
659 0493(1989)117<2113:APOHLS>2.0.CO;2

660 Avissar, R., & Schmidt, T. (1998). An evaluation of the scale at which ground-surface heat flux
661 patchiness affects the convective boundary layer using large-eddy simulations. *Journal of the*
662 *Atmospheric Sciences*, *55*, 2666–2689. https://doi.org/10.1175/1520-
663 0469(1998)055<2666:AEOTSA>2.0.CO;2

Baik, J. J., Kim, Y. H., & Chun, H. Y. (2001). Dry and moist convection forced by an urban heat island. *Journal of Applied Meteorology*, *40*(8), 1462–1475. https://doi.org/10.1175/1520-0450(2001)040<1462:DAMCFB>2.0.CO;2

Berg, L. K., & Stull, R. B. (2005). A simple parameterization coupling the convective daytime boundary layer and fair-weather cumuli. *Journal of the Atmospheric Sciences*, *62*(6), 1976–1988. https://doi.org/10.1175/JAS3437.1

Bou-Zeid, E., Anderson, W., Katul, G. G., & Mahrt, L. (2020). The persistent challenge of surface heterogeneity in boundary-layer meteorology: A review. *Boundary-Layer Meteorology*, *177*, 227–245. https://doi.org/10.1007/s10546-020-00551-8

Brunsell, N. A., Mechem, D. B., & Anderson, M. C. (2011). Surface heterogeneity impacts on boundary layer dynamics via energy balance partitioning. *Atmospheric Chemistry and Physics*, *11*, 3403–3416. https://doi.org/10.5194/acp-11-3403-2011

Chaney, N. W., Metcalfe, P., & Wood, E. F. (2016). HydroBlocks: a field-scale resolving land surface model for application over continental extents. *Hydrological Processes*, *30*(20), 3543–3559. https://doi.org/https://doi.org/10.1002/hyp.10891

Cheng, Y., Chan, P. W., Wei, X., Hu, Z., Kuang, Z., & McColl, K. A. (2021). Soil moisture control of precipitation reevaporation over a heterogeneous land surface. *Journal of the Atmospheric Sciences*, *78*(10), 3369–3383. https://doi.org/10.1175/JAS-D-21-0059.1

Cioni, G., & Hohenegger, C. (2018). A simplified model of precipitation enhancement over a heterogeneous surface. *Hydrology and Earth System Sciences*, *22*(6), 3197–3212. https://doi.org/10.5194/hess-22-3197-2018

Dai, Y., Zeng, X., Dickinson, R. E., Baker, I., Bonan, G. B., Bosilovich, M. G., et al. (2003). The common land model experience. *Bulletin of the American Meteorological Society*, 84(8), 1013–1024. https://doi.org/https://doi.org/10.1175/BAMS-84-8-1013

Dirmeyer, P. A., Balsamo, G., Blyth, E. M., Morrison, R., & Cooper, H. M. (2021). Land-Atmosphere Interactions Exacerbated the Drought and Heatwave Over Northern Europe During Summer 2018. *AGU Advances*, *2*(2), 1–16. https://doi.org/10.1029/2020av000283

Dixon, P. G., & Mote, T. L. (2003). Patterns and causes of Atlanta's urban heat island-initiated precipitation. *Journal of Applied Meteorology*, *42*(9), 1273–1284. https://doi.org/10.1175/1520-0450(2003)042<1273:PACOAU>2.0.CO;2

Doran, J. C., Shaw, W. J., & Hubbe, J. M. (1995). Boundary layer characteristics over areas of inhomogeneous surface fluxes. *Journal of Applied Meteorology*, *34*, 559–571. https://doi.org/https://doi.org/10.1175/1520-0450-34.2.559

Fischer, E. M., Seneviratne, S. I., Lüthi, D., & Schär, C. (2007). Contribution of land-atmosphere coupling to recent European summer heat waves. *Geophysical Research Letters*, *34*(6), 1–6. https://doi.org/10.1029/2006GL029068

Fowler, M. D., Neale, R. B., Simon, J. S., Lawrence, D. M., Chaney, N. W., Dirmeyer, P. A., et al. (2022, November). Assessing the atmospheric response to subgrid surface heterogeneity in CESM2 - code, output, and analysis script [Dataset]. *Zenodo*. https://doi.org/10.5281/zenodo.7308152

Gettelman, A., Truesdale, J. E., Bacmeister, J. T., Caldwell, P. M., Neale, R. B., Bogenschutz, P.

A., & Simpson, I. R. (2019). The Single Column Atmosphere Model Version 6 (SCAM6): Not a scam but a tool for model evaluation and development. *Journal of Advances in Modeling Earth Systems*, *11*(5), 1381–1401. https://doi.org/10.1029/2018MS001578

Golaz, J. C., Larson, V. E., & Cotton, W. R. (2002). A PDF-based model for boundary layer clouds. Part I: Method and model description. *Journal of the Atmospheric Sciences*, *59*, 3540–3551. https://doi.org/10.1175/1520-0469(2002)059<3540:APBMFB>2.0.CO;2

Graf, M., Arnault, J., Fersch, B., & Kunstmann, H. (2021). Is the soil moisture precipitation feedback enhanced by heterogeneity and dry soils? A comparative study. *Hydrological Processes*, *35*(9), 1–15. https://doi.org/10.1002/hyp.14332

Gustafson, W. I., Vogelmann, A. M., Cheng, X., Dumas, K. K., Endo, S., Johnson, K. L., et al. (2019). *Description of the LASSO data bundles product*. https://doi.org/10.2172/1469590

Hahmann, A. N., & Dickinson, R. E. (2001). A fine-mesh land approach for general circulation models and its impact on regional climate. *Journal of Climate*, 14(7), 1634–1646. https://doi.org/10.1175/1520-0442(2001)014<1634:AFMLAF>2.0.CO;2

Hirschi, M., Seneviratne, S. I., Alexandrov, V., Boberg, F., Boroneant, C., Christensen, O. B., et al. (2011). Observational evidence for soil-moisture impact on hot extremes in southeastern Europe. *Nature Geoscience*, *4*, 17–21. https://doi.org/10.1038/ngeo1032

Hjelmfelt, M. R. (1982). Numerical simulation of the effects of St. Louis on mesoscale boundary-layer airflow and vertical air motion: Simulations of urban vs. non-urban effects. *Journal of Applied Meteorology*, *21*, 1239–1257. https://doi.org/https://doi.org/10.1175/1520-0450(1982)021%3C1239:NSOTEO%3E2.0.CO;2

Huang, H. Y., & Margulis, S. A. (2013). Impact of soil moisture heterogeneity length scale and gradients on daytime coupled land-cloudy boundary layer interactions. *Hydrological Processes*, *27*, 1988–2003. https://doi.org/10.1002/hyp.9351

Huang, M., Ma, P.-L., Chaney, N. W., Hao, D., Bisht, G., Fowler, M. D., et al. (2022). Representing surface heterogeneity in land-atmosphere coupling in E3SMv1 single-column model over ARM SGP during summertime. *Geoscientific Model Development Discussions*, *2022*, 1–20. https://doi.org/10.5194/gmd-2021-421

Hubbe, J. M., Doran, J. C., Liljegren, J. C., & Shaw, W. J. (1997). Observations of spatial variations of boundary layer structure over the southern great plains cloud and radiation testbed. *Journal of Applied Meteorology*, *36*(9), 1221–1231. https://doi.org/10.1175/1520-0450(1997)036<1221:OOSVOB>2.0.CO;2

Kang, S. L. (2016). Regional bowen ratio controls on afternoon moist convection: A large eddy simulation study. *Journal of Geophysical Research: Atmospheres*, *121*, 14,056-14,083. https://doi.org/10.1002/2016JD025567

Koster, R. D., & Suarez, M. J. (1992). Modeling the land surface boundary in climate models as a composite of independent vegetation stands. *Journal of Geophysical Research*, 97(D3), 2697–2715. https://doi.org/10.1029/91JD01696

Kustas, W. P., & Albertson, J. D. (2003). Effects of surface temperature contrast on land-atmosphere exchange: A case study from Monsoon 90. *Water Resources Research*, *39*, 1–11. https://doi.org/10.1029/2001WR001226

Larson, V. E. (2017). CLUBB-SILHS: A parameterization of subgrid variability in the atmosphere. arXiv. https://doi.org/10.48550/ARXIV.1711.03675

Larson, V. E., Golaz, J. C., & Cotton, W. R. (2002). Small-scale and mesoscale variability in cloudy boundary layers: Joint probability density functions. *Journal of the Atmospheric Sciences*, *59*(24), 3519–3539. https://doi.org/10.1175/1520-0469(2002)059<3519:SSAMVI>2.0.CO;2

Lawrence, D. M., Fisher, R. A., Koven, C. D., Oleson, K. W., Swenson, S. C., Bonan, G., et al. (2019). The Community Land Model Version 5: Description of new features, benchmarking, and impact of forcing uncertainty. *Journal of Advances in Modeling Earth Systems*, *11*(12), 4245–4287. https://doi.org/10.1029/2018MS001583

Li, D., Bou-Zeid, E., Barlage, M., Chen, F., & Smith, J. A. (2013). Development and evaluation of a mosaic approach in the WRF-Noah framework. *Journal of Geophysical Research Atmospheres*, *118*(21), 11,918-11,935. https://doi.org/10.1002/2013JD020657

Machulskaya, E., & Mironov, D. (2018). Boundary conditions for scalar (co)variances over heterogeneous surfaces. *Boundary-Layer Meteorology*, *169*, 139–150. https://doi.org/10.1007/s10546-018-0354-6

Mahrt, L. (2000). Surface heterogeneity and vertical structure of the boundary layer. *Boundary-Layer Meteorology*, *96*, 33–62. https://doi.org/10.1023/A:1002482332477

Mocko, D. M., Kumar, S. V., Peters-Lidard, C. D., & Wang, S. (2021). Assimilation of vegetation conditions improves the representation of drought over agricultural areas. *Journal of Hydrometeorology*, *22*(5), 1085–1098. https://doi.org/10.1175/JHM-D-20-0065.1

Neale, R. B., Richter, J. H., & Jochum, M. (2008). The impact of convection on ENSO: From a delayed oscillator to a series of events. *Journal of Climate*, *21*(22), 5904–5924. https://doi.org/10.1175/2008JCLI2244.1

Ookouchi, Y., Segal, M., Kessler, R. C., & Pielke, R. A. (1984). Evaluation of soil moisture effects on the generation and modification of mesoscale circulations. *Monthly Weather Review*, *112*. https://doi.org/10.1175/1520-0493(1984)112,2281:EOSMEO.2.0.CO;2

Pielke Sr., R. A. (2001). Influence of the spatial distribution of vegetation and soils on the prediction of cumulus convective rainfall. *Reviews of Geophysics*, *39*, 151–177. https://doi.org/doi:10.1029/1999RG000072

Ramos da Silva, R., Gandu, A. W., Sá, L. D. A., & Dias, M. A. F. S. (2011). Cloud streets and land-water interactions in the Amazon. *Biogeochemistry*, *105*(1), 201–211. https://doi.org/10.1007/s10533-011-9580-4

Rieck, M., Hohenegger, C., & van Heerwaarden, C. C. (2014). The influence of land surface heterogeneities on cloud size development. *Monthly Weather Review*, *142*(10), 3830–3846. https://doi.org/10.1175/MWR-D-13-00354.1

Santanello, J. A., Roundy, J., & Dirmeyer, P. A. (2015). Quantifying the land-atmosphere coupling behavior in modern reanalysis products over the U.S. southern great plains. *Journal of Climate*, *28*(14), 5813–5829. https://doi.org/10.1175/JCLI-D-14-00680.1

Schrieber, K., Stull, R., & Zhang, Q. (1996). Distributions of surface-layer buoyancy versus lifting condensation level over a heterogeneous land surface. *Journal of the Atmospheric Sciences*, *53*, 1086–1107. https://doi.org/https://doi.org/10.1175/1520-

0469(1996)053%3C1086:DOSLBV%3E2.0.CO;2

Shem, W., & Shepherd, M. (2009). On the impact of urbanization on summertime thunderstorms in Atlanta: Two numerical model case studies. *Atmospheric Research*, *92*(2), 172–189. https://doi.org/10.1016/j.atmosres.2008.09.013

Shepherd, J. M. (2005). A review of current investigations of urban-induced rainfall and recommendations for the future. *Earth Interactions*, *9*(12). https://doi.org/10.1175/EI156.1

Simon, J.S., Bragg, A. D., Chaney, N.W. (2022). Spatial organization of surface fluxes leads to appreciable impacts in the development of shallow convection. Manuscript in preperation for submission to *Geophysical Research Letters*.

Simon, J. S., Bragg, A. D., Dirmeyer, P. A., & Chaney, N. W. (2021). Semi-coupling of a field-scale resolving Land-surface model and WRF-LES to investigate the influence of land-surface heterogeneity on cloud development. *Journal of Advances in Modeling Earth Systems*, *13*. https://doi.org/10.1029/2021MS002602

Skamarock, W. C., Klemp, J. B., Dudhia, J., Gill, D. O., Barker, D. M., Wang, W., & Powers, J. G. (2005). *A description of the advanced research WRF version 2*. (NCAR/TN-475+STR). NCAR Technical Note.

Swenson, S. C., Clark, M., Fan, Y., Lawrence, D. M., & Perket, J. (2019). Representing intrahillslope lateral subsurface flow in the Community Land Model. *Journal of Advances in Modeling Earth Systems*, *11*(12), 4044–4065. https://doi.org/10.1029/2019MS001833

Taylor, C. M., Gounou, A., Guichard, F., Harris, P. P., Ellis, R. J., Couvreux, F., & De Kauwe, M. (2011). Frequency of sahelian storm initiation enhanced over mesoscale soil-moisture patterns. *Nature Geoscience*, *4*(7), 430–433. https://doi.org/10.1038/ngeo1173

Zhang, G. J., & McFarlane, N. A. (1995). Sensitivity of climate simulations to the parameterization of cumulus convection in the canadian climate centre general circulation model. *Atmosphere - Ocean*, *33*(3), 407–446. https://doi.org/10.1080/07055900.1995.9649539

Zhang, Y., Huang, Q., Ma, Y., Luo, J., Wang, C., Li, Z., & Chou, Y. (2021). Large eddy simulation of boundary-layer turbulence over the heterogeneous surface in the source region of the Yellow River. *Atmospheric Chemistry and Physics*, *21*(20), 15949–15968. https://doi.org/10.5194/acp-21-15949-2021